PHILOSOPHICAL TRANSACTIONS A

rsta.royalsocietypublishing.org

Research

Cite this article: Yevick A, Evans DJ, Grier DG. 2017 Photokinetic analysis of the forces and torques exerted by optical tweezers carrying angular momentum. *Phil. Trans. R. Soc. A* **375**: 20150432.
http://dx.doi.org/10.1098/rsta.2015.0432

Accepted: 31 August 2016

One contribution of 14 to a theme issue 'Optical orbital angular momentum'.

Subject Areas:
optics, materials science

Keywords:
optical trapping, angular momentum, spin-curl force, Brownian vortex

Author for correspondence:
David G. Grier
e-mail: david.grier@nyu.edu

Photokinetic analysis of the forces and torques exerted by optical tweezers carrying angular momentum

Aaron Yevick, Daniel J. Evans and David G. Grier

Department of Physics, and Center for Soft Matter Research, New York University, New York, NY 10003, USA

DGG, 0000-0002-4382-5139

The theory of photokinetic effects expresses the forces and torques exerted by a beam of light in terms of experimentally accessible amplitude and phase profiles. We use this formalism to develop an intuitive explanation for the performance of optical tweezers operating in the Rayleigh regime, including effects arising from the influence of light's angular momentum. First-order dipole contributions reveal how a focused beam can trap small objects, and what features limit the trap's stability. The first-order force separates naturally into a conservative intensity-gradient term that forms a trap and a non-conservative solenoidal term that drives the system out of thermodynamic equilibrium. Neither term depends on the light's polarization; light's spin angular momentum plays no role at dipole order. Polarization-dependent effects, such as trap-strength anisotropy and spin-curl forces, are captured by the second-order dipole-interference contribution to the photokinetic force. The photokinetic expansion thus illuminates how light's angular momentum can be harnessed for optical micromanipulation, even in the most basic optical traps.

This article is part of the themed issue 'Optical orbital angular momentum'.

1. Introduction

The intrinsic spin angular momentum carried by circularly polarized light can be transferred directly to an optically anisotropic object, which then experiences a tangible torque [1]. The discovery a quarter-century

THE ROYAL SOCIETY PUBLISHING

ago [2] that some modes of light also carry orbital angular momentum created a revolution in optical micromanipulation because this form of angular momentum can be transferred directly to isotropic and anisotropic objects alike [3–7]. The orbital angular momentum content of a wave is governed by phase gradients, rather than spatial variations in the polarization, and thus is very amenable to experimental control. Considerable attention therefore has been devoted to harnessing the forces and torques arising from phase gradients in specially structured beams of light [8].

The distinction between spin angular momentum and orbital angular momentum becomes blurred in strongly focused beams of light, because gradients of the polarization couple to gradients in the phase through Maxwell's equations. The resulting spin-to-orbital conversion [9–11] provides a subtle mechanism for light's spin to influence the motion of optically isotropic particles [12]. This mechanism vanishes, however, in paraxial beams of light.

Recently, an alternative avenue for spin-dependent micromanipulation has been identified [13–15] that is based on forces arising from the curl of the spin angular momentum density. Unlike spin-to-orbit conversion, this mechanism operates even in collimated beams of light [16,17].

The forces and torques exerted by any beam of light on any illuminated object can be computed with the Lorenz–Mie theory of light scattering and its generalizations [18,19]. These numerical techniques, however, do not inherently distinguish how distinct characteristics of a beam of light contribute to different features of the force and torque landscape. To elucidate these relationships, we apply the theory of photokinetic effects [17] to a simple yet useful model system: the single-beam optical traps conventionally known as optical tweezers [20]. The results of this analysis apply quantitatively in the Rayleigh limit, for objects substantially smaller than the wavelength of light. More generally, this approach provides guidance for optimizing the design and operation of optical traps.

2. Fields in optical tweezers

We describe an optical tweezer as a focused monochromatic Gaussian beam propagating along $\hat{z}$ with frequency ω and uniform polarization $\hat{\epsilon}$. The light's electric field may then be written in cylindrical coordinates, $\mathbf{r} = (r, \theta, z)$, as [21]

$$\mathbf{E}(\mathbf{r}, t) = u(\mathbf{r})\, \mathrm{e}^{\mathrm{i}\phi(\mathbf{r})}\, \mathrm{e}^{-\mathrm{i}\omega t} \hat{\epsilon}, \tag{2.1a}$$

with amplitude profile

$$u(\mathbf{r}) = u_0 \frac{z_\mathrm{R}}{\sqrt{z^2 + z_\mathrm{R}^2}} \exp\left(-\frac{r^2}{w_0^2} \frac{z_\mathrm{R}^2}{z^2 + z_\mathrm{R}^2} \right) \tag{2.1b}$$

and phase profile

$$\phi(\mathbf{r}) = kz + \frac{1}{2} k \frac{zr^2}{z^2 + z_\mathrm{R}^2} - \tan^{-1}\left(\frac{z}{z_\mathrm{R}} \right), \tag{2.1c}$$

where $k = n_\mathrm{m}\omega/c$ is the wavenumber of light in a medium of refractive index n_m and w_0 is the diameter of the beam's waist at best focus in the plane $z = 0$. The Rayleigh range, $z_\mathrm{R} = \frac{1}{2} k w_0^2$, characterizes how sharply the beam is focused. A Gaussian beam's cross-sectional area doubles over this distance.

In an optical train that is free of geometric aberrations, the diameter of the beam's waist is related to the numerical aperture (NA) of the lens that brings the light to a focus by

$$w_0 \approx \frac{2\pi}{n_\mathrm{m} k\, \mathrm{NA}}. \tag{2.2}$$

In the same approximation, the Rayleigh range is related to the numerical aperture by

$$k z_\mathrm{R} \approx \frac{2\pi^2}{n_\mathrm{m}^2\, \mathrm{NA}^2}. \tag{2.3}$$

3. Photokinetic effects at dipole order

(a) Electric dipole forces

The light's electric field induces an oscillating electric dipole moment in an illuminated particle located at position $\mathbf{r}$,

$$\mathbf{p}(\mathbf{r},t) = \alpha_\mathrm{e}\mathbf{E}(\mathbf{r},t), \tag{3.1}$$

where α_e is the object's complex dipole polarizability. The polarizability of a dielectric particle of refractive index n_p whose radius a_p is smaller than the wavelength of light, $ka_\mathrm{p} < 1$, is given approximately by [22,23]

$$\alpha_\mathrm{e} = \frac{\alpha_\mathrm{e}^{(0)}}{1 - [\mathrm{i}/(6\pi\epsilon_0 n_\mathrm{m}^2)]k^3\alpha_\mathrm{e}^{(0)}}, \tag{3.2a}$$

where the Clausius–Mossotti polarizability is

$$\alpha_\mathrm{e}^{(0)} = 4\pi\epsilon_0 n_\mathrm{m}^2 a_\mathrm{p}^3 \frac{n_\mathrm{p}^2 - n_\mathrm{m}^2}{n_\mathrm{p}^2 + 2n_\mathrm{m}^2} \tag{3.2b}$$

and where ϵ_0 is the vacuum permittivity. The sign of $\alpha_\mathrm{e}^{(0)}$ depends on whether the particle has a higher refractive index than the medium. This, in turn, determines the sign of the real part of α_e; the imaginary part is always positive.

The time-averaged Lorentz force acting on this induced dipole moment is [24]

$$\mathbf{F}_\mathrm{e}(\mathbf{r}) = \tfrac{1}{2}\,\Re\{p(\mathbf{r},t)\nabla E^*(\mathbf{r},t)\}, \tag{3.3}$$

where $\Re\{\cdot\}$ represents the real part of its argument. This contribution to the optical force can be expressed in terms of the field's amplitude and phase profiles as [15,17]

$$\mathbf{F}_\mathrm{e}(\mathbf{r}) = \tfrac{1}{4}\alpha_\mathrm{e}'\nabla u^2(\mathbf{r}) + \tfrac{1}{2}\alpha_\mathrm{e}'' u^2(\mathbf{r})\nabla\phi(\mathbf{r}), \tag{3.4}$$

where α_e' and α_e'' are the real and imaginary parts of α_e, respectively. The first term on the right-hand side of equation (3.4) is the manifestly conservative intensity-gradient force responsible for trapping the object. The second describes a force that does not conserve mechanical energy and so contributes to the radiation pressure [8,15,17]. This distinction may be appreciated because $\nabla \times [u^2(\mathbf{r})\nabla\phi(\mathbf{r})] \neq 0$ in general, so that the second term cannot be expressed as the gradient of a potential. The competing influences of conservative and non-conservative optical forces were identified in the original description of optical tweezers [20]. Reformulating the theory in terms of the beam's amplitude and phase profiles affords a clear interpretation of their origin.

Substituting the optical tweezer's field from equation (2.1) into the expression for the photokinetic force in equation (3.4) yields

$$\begin{aligned}\frac{\mathbf{F}_\mathrm{e}(\mathbf{r})}{F_0(\mathbf{r})} = &-\left(1 - \frac{\alpha_\mathrm{e}''}{\alpha_\mathrm{e}'}\frac{z}{z_\mathrm{R}}\right)\frac{r}{z_\mathrm{R}}\hat{r} - \left(\frac{1}{kz_\mathrm{R}} - \frac{r^2}{z^2 + z_\mathrm{R}^2}\right)\frac{z}{z_\mathrm{R}}\hat{z} \\ &+ \frac{\alpha_\mathrm{e}''}{\alpha_\mathrm{e}'}\left[1 - \frac{1}{kz_\mathrm{R}} + \frac{z^2}{z_\mathrm{R}^2} - \frac{1}{2}\frac{z^2 - z_\mathrm{R}^2}{z^2 + z_\mathrm{R}^2}\frac{r^2}{z_\mathrm{R}^2}\right]\hat{z},\end{aligned} \tag{3.5a}$$

where the force scale is set by

$$F_0(\mathbf{r}) = \frac{1}{2}k\alpha_\mathrm{e}'\frac{z_\mathrm{R}^2}{z^2 + z_\mathrm{R}^2}u^2(\mathbf{r}). \tag{3.5b}$$

Figure 1 shows typical streamlines of $\mathbf{F}_\mathrm{e}(\mathbf{r})$. No force acts on index-matched particles, for which $\alpha_\mathrm{e}' = 0$. The overall sign of $\mathbf{F}_\mathrm{e}(\mathbf{r})$ similarly depends on the particle's refractive index relative to that of the medium.

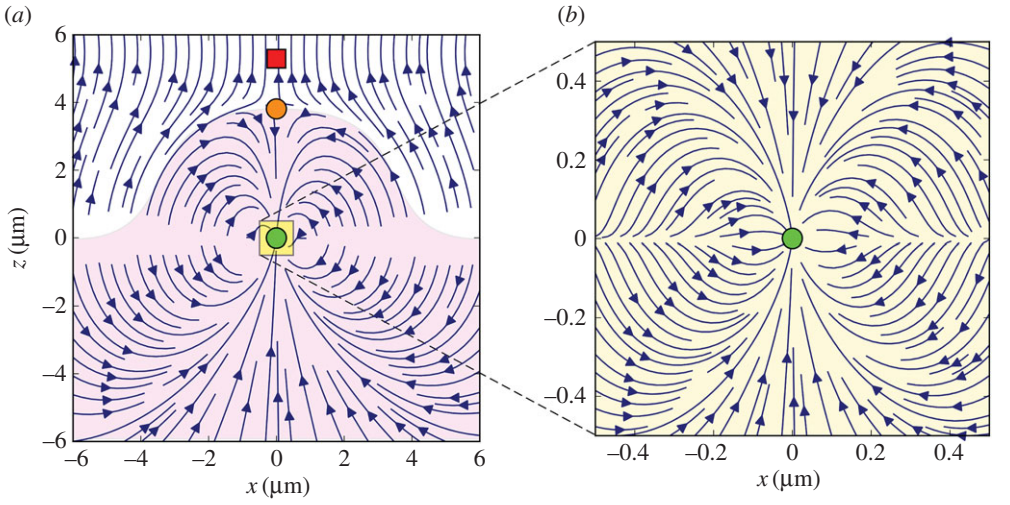

Figure 1. Streamlines in the plane $y = 0$ of the total dipole force acting on a 100 nm diameter silica sphere in water, computed as a superposition of $\mathbf{F}_e(\mathbf{r})$ from equation (3.5) and the analogous result for the magnetic dipole contribution, $\mathbf{F}_m(\mathbf{r})$. (*a*) Large-scale view. The central (green) circle identifies the stable equilibrium at z_- from equation (3.8). The other (orange) circle identifies z_+. The (red) square identifies the point of marginal radial stability, z_c, from equation (3.7). The (purple) shaded region denotes the domain of stable trapping. (*b*) Region of interest corresponding to the (yellow) shaded region at the center of (*a*) showing the detailed structure of the force field. The force field pulls the particle inward toward the trap from all directions. Unstable points are out of the field of view. (Online version in colour.)

(i) Small displacements: Hookean trap

For particles that are confined near the origin, the first-order photokinetic force reduces to a Hookean restoring force,

$$\lim_{r,z\to 0} \mathbf{F}_e(\mathbf{r}) = -\frac{1}{2}k\alpha_e'\left[\frac{r}{z_R}\hat{r} + \frac{(z-z_0)}{kz_R^2}\hat{z}\right], \tag{3.6a}$$

with an axial offset,

$$z_0 = \frac{\alpha_e''}{\alpha_e'} z_R(kz_R - 1), \tag{3.6b}$$

arising from radiation pressure. This offset itself is small compared with the wavelength of light because $\alpha_e'' \ll \alpha_e'$ for small particles.

At this level of approximation, the force exerted by an optical trap conserves mechanical energy. It transfers no angular momentum and exerts no torques. A trapped colloidal particle therefore comes into thermodynamic equilibrium with the surrounding fluid, and fluctuates in place. Observing departures from equilibrium requires either larger-scale displacements or a mechanism for transferring light's angular momentum to the trapped particle. Both dipole-order departures from equilibrium and higher-order polarization-dependent torques are discussed below.

Assuming the particle is trapped near the focal point at the origin of the coordinate system, the radial stiffness of the trap exceeds the axial stiffness by a factor of kz_R. The inherent anisotropy between in-plane and axial trapping strength has been observed experimentally [25–28] and has been discussed in the theoretical literature [27,29]. Referring to equation (2.3), the stiffness anisotropy of a trap focused into water by a lens with numerical aperture NA = 1.2 should be 7.7, which agrees well with the measured value of 7.1 reported for a polystyrene sphere of radius $a_p = 0.11\,\mu$m in optical tweezers at a vacuum wavelength of 1064 nm [27].

(ii) Stable and unstable equilibria

Although a trap's axial stability might appear to limit its practical range, its radial stability also limits its ability to capture particles by pulling them inward toward the focus. The radial component of $\mathbf{F}_e(\mathbf{r})$ vanishes along the axis, $r = 0$. The radial component of $\mathbf{F}_e(\mathbf{r})$ from equation (3.5*a*) reveals that this line of radial equilibria is stable only for axial positions z less than

$$z_c = z_R \frac{\alpha_e'}{\alpha_e''} = \frac{3}{2} \frac{z_R}{k^3 a_p^3} \frac{n_p^2 + 2n_m^2}{n_p^2 - n_m^2}. \tag{3.7}$$

The trap is radially unstable downstream of $z = z_c$ for both high- and low-index particles. This loss of radial confinement inherently limits the axial range over which optical tweezers can capture small objects. Equation (2.3) then suggests that increasing NA reduces z_c and thus restricts the range over which a trap can acquire its target.

The full expression for $\mathbf{F}_e(\mathbf{r})$ features two points of mechanical equilibrium along the optical axis:

$$z_\pm = \frac{1}{2k} \left[\frac{\alpha_e'}{\alpha_e''} \pm \sqrt{\left(\frac{\alpha_e'}{\alpha_e''}\right)^2 - 4kz_R(kz_R - 1)} \right], \tag{3.8}$$

with the positive choice representing an unstable equilibrium and the negative choice representing the location of the trap. These solutions exist only for particles satisfying

$$\frac{1}{k^3 a_p^3} \frac{n_p^2 + 2n_m^2}{n_p^2 - n_m^2} > \frac{4\pi}{3} \frac{1}{n_m \mathrm{NA}} \sqrt{\left(\frac{2\pi}{n_m \mathrm{NA}}\right)^2 - 2}. \tag{3.9}$$

Other particles are repelled from the focus. This condition for stable trapping favours using high-NA lenses, particularly for small, high-index particles. The stable trapping solution, z_-, reduces to the linear solution, z_0, in the limit that $\alpha_e'' < \alpha_e'$.

(iii) Non-conservative forces and angular momentum

The full expression for $\mathbf{F}_e(\mathbf{r})$ includes a non-conservative part that contributes to the curl of the force,

$$\nabla \times \mathbf{F}_e(\mathbf{r}) = 2F_0(\mathbf{r}) \frac{\alpha_e''}{\alpha_e'} \frac{kr}{z_R} \left(1 - \frac{1}{kz_R} + \frac{1}{2} \frac{r^2}{z^2 + z_R^2}\right) \hat{\theta}. \tag{3.10}$$

The solenoidal component of $\mathbf{F}_e(\mathbf{r})$ tends to bias the thermal fluctuations of a trapped colloidal particle into a toroidal roll that circulates in the same sense as $\nabla \times \mathbf{F}_e(\mathbf{r})$. Such Brownian vortex circulation has been observed experimentally [30–32] and analysed theoretically [33,34].

Figure 2 illustrates Brownian vortex circulation in the first-order force field of an optical tweezer described by equation (3.5). A small particle trapped near the focus of the Gaussian beam is displaced by random thermal forces away from its point of mechanical equilibrium and into the non-conservative force field. Over time, or in an ensemble average, its trajectory circulates around a vortex core that is indicated by a dashed circle in figure 2*a*. The streamlines plotted in figure 2 trace out the computed Brownian vortex circulation [34] of a 100 nm diameter silica sphere diffusing in water under the influence of a strongly focused optical trap. It should be emphasized that this circulation represents a bias of a few per cent on the otherwise random Brownian motion, and is only seen experimentally with extensive time averaging.

The circulating probability current of the trapped particle is associated with an angular momentum density that the light imparts to the mechanical system independent of its polarization or phase profile. This angular momentum arises from transfer of linear momentum from the non-uniform beam of light and is directed transverse to the optical axis. Because the vortex core forms a closed loop, the system's total angular momentum vanishes, as expected.

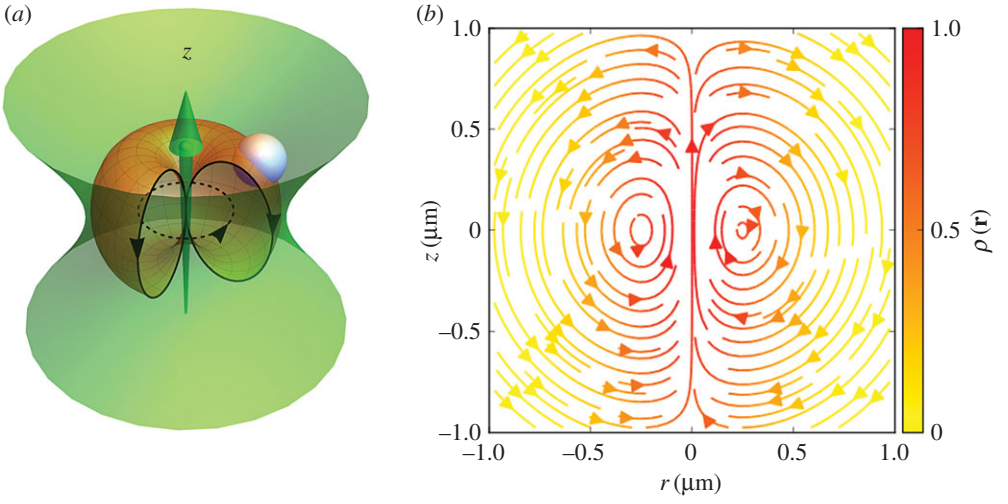

Figure 2. Brownian vortex circulation of a colloidal particle in an optical tweezer. (*a*) Schematic of the geometry. A colloidal sphere diffuses near the focus of a Gaussian beam propagating along $\hat{z}$. The sphere's Brownian motion is biased into a toroidal roll whose core is represented by the horizontal dashed circle. (*b*) Computed streamlines of the ensemble- or time-averaged probability flux of a 100 nm diameter silica sphere diffusing in an optical trap. The radial cylindrical coordinate is reflected about $\hat{z}$ to illustrate the toroidal geometry. Colours represent the relative probability density for finding the particle, which is peaked near the origin at the position of the trap. (Online version in colour.)

Brownian vortex circulation is interesting principally as a manifestation of a largely overlooked class of stochastic machines. Brownian vortexes differ from conventional deterministic machines in that they do nothing at all in the absence of noise. They are also different from other noisy machines, such as thermal ratchets and Brownian motors, whose motive force fields are time-dependent. The force field that drives a Brownian vortex is static.

Still more remarkably, the number of toroidal rolls and their direction of circulation need not simply follow the direction of the non-conservative force. The competition between advection and diffusion in such systems can cause topological transitions and flux reversals in the pattern of circulation [31,33,34]. Such exotic phenomena arise when the non-conservative component of the force fields has a projection onto the conservative component that changes sign with position [34]. The electric dipole force from equation (3.5) is too simple for this. The more exotic features of Brownian vortex circulation require the higher-order corrections to $\mathbf{F}_{\mathrm{e}}(\mathbf{r})$ that arise for larger particles [31,34].

(b) Magnetic dipole forces

The light's magnetic field also contributes to photokinetic forces, even for purely dielectric particles. Surface currents associated with the oscillating induced electric dipole not only couple directly to the magnetic field through the standard Lorentz force [35], but also contribute to the magnetic polarizability, α_{m}, through field-induced distortions. The result is a time-averaged magnetic dipole force $\mathbf{F}_{\mathrm{m}}(\mathbf{r})$ that is term-for-term analogous to equation (3.4).

The magnetic field's amplitude and phase profiles are related to those of the electric field through the Maxwell–Faraday equation

$$\mathbf{B}(\mathbf{r},t) = -\frac{\mathrm{i}}{\omega}\nabla\times\mathbf{E}(\mathbf{r},t) \tag{3.11a}$$

$$= \sum_{j=1}^{3} B_j(\mathbf{r})\mathrm{e}^{-\mathrm{i}\omega t}\hat{\epsilon}_j \tag{3.11b}$$

for monochromatic light, where μ is the permeability of the medium. Substituting equation (2.1) into equation (3.11) yields

$$\mathbf{B}(\mathbf{r},t) = \frac{1}{c}\, u(\mathbf{r})\, \mathrm{e}^{\mathrm{i}\phi(\mathbf{r})}\, \mathrm{e}^{-\mathrm{i}\omega t} \left[b(\mathbf{r})\, \hat{\epsilon}_\mathrm{m} + \frac{y}{z - \mathrm{i}z_\mathrm{R}} \hat{z} \right], \tag{3.12}$$

where $\hat{\epsilon}_\mathrm{m} = \hat{z} \times \hat{\epsilon}$ and where

$$b(\mathbf{r}) = 1 - \frac{1}{k(z_\mathrm{R} + \mathrm{i}z)} + \frac{r^2}{2(z_\mathrm{R} + \mathrm{i}z)^2}. \tag{3.13}$$

The additional transverse structure described by equation (3.13) and the axial component of the magnetic field both vanish in the paraxial approximation. Together, equations (2.1) and (3.12) describe a Gaussian TEM_{00} mode in the paraxial limit.

The magnetic dipole contribution to the photokinetic force has the same functional form as the electric dipole contribution. Because $\alpha''_\mathrm{m}/\alpha'_\mathrm{m}$ need not be equal to $\alpha''_\mathrm{e}/\alpha'_\mathrm{e}$, however, the magnetic contribution tends to displace the equilibrium point and critical point. This displacement is small for a dielectric particle, but can be substantial for a magneto-dielectric particle [36].

As a concrete example, a 100 nm diameter silica sphere in room-temperature water has $\alpha''_\mathrm{e}/\alpha'_\mathrm{m} = 0.018$ at $\lambda = 532$ nm, and $\alpha''_\mathrm{m}/\alpha'_\mathrm{m} = 0.001$. According to equation (3.6*b*), the electric-dipole contribution to the displacement is 10% of the Rayleigh range in a diffraction-limited trap. The additional displacement due to magnetic dipole forces amounts to just 7% of that. The equivalent calculation for a chromium sphere, $n_\mathrm{p} = 3.0343 + 3.3300\mathrm{i}$, yields $\alpha''_\mathrm{e}/\alpha'_\mathrm{m} = 0.98$ and $\alpha''_\mathrm{m}/\alpha'_\mathrm{m} = -1.13$. The magnetic contribution not only has a larger magnitude than the electric, but also reverses the sign of the offset.

4. Angular momentum and higher-order photokinetic effects

As for the electric dipole force, the magnetic dipole force does not depend on the light's state of polarization. There is ample evidence, however, that polarization influences optical tweezers' trapping characteristics. Linearly polarized optical tweezers are measurably stiffer along the axis of polarization [27,29,37], an effect that is not captured by equation (3.5). Circularly polarized tweezers are observed to exert transverse forces that are not present in linearly polarized optical tweezers [13]. Such polarization-dependent effects emerge at higher order in the photokinetic expansion and provide mechanisms for light's angular momentum to influence the motion of trapped objects.

Interference between electric and magnetic dipole scattering gives rise to a second-order photokinetic force [36],

$$\mathbf{F}_\mathrm{em}(\mathbf{r}) = -\frac{k^4}{12\pi\epsilon_0 c} \Re\{\alpha_\mathrm{e}\alpha^*_\mathrm{m}\mathbf{E}(\mathbf{r},t) \times \mathbf{B}^*(\mathbf{r},t)\}. \tag{4.1}$$

Expressed in terms of the amplitude and phase of a scalar field [17],

$$\mathbf{F}_\mathrm{em}(\mathbf{r},t) = \frac{\epsilon k^3}{24\pi\epsilon_0} \Im\{\alpha_\mathrm{e}\alpha^*_\mathrm{m}\} \nabla u^2(\mathbf{r}) \tag{4.2a}$$

$$- \frac{\epsilon k^3}{12\pi\epsilon_0} \Re\{\alpha_\mathrm{e}\alpha^*_\mathrm{m}\} u^2(\mathbf{r}) \nabla\phi(\mathbf{r}) \tag{4.2b}$$

$$- \frac{\epsilon k^3}{12\pi\epsilon_0} \Im\{\alpha_\mathrm{e}\alpha^*_\mathrm{m}\} \nabla \cdot \mathrm{T}^{(\mathrm{s})}(\mathbf{r}) \tag{4.2c}$$

$$- \frac{\epsilon k^3}{12\pi\epsilon_0} \Re\{\alpha_\mathrm{e}\alpha^*_\mathrm{m}\} \nabla \cdot \mathrm{T}^{(\mathrm{a})}(\mathbf{r}), \tag{4.2d}$$

where

$$\mathrm{T}^{(\mathrm{s})}(\mathbf{r}) = u^2(\mathbf{r}) \begin{bmatrix} \epsilon_x^2 \cos\delta & 0 & 0 \\ 0 & \epsilon_y^2 \cos\delta & 0 \\ 0 & 0 & 0 \end{bmatrix} \tag{4.3a}$$

and

$$\mathcal{T}^{(\mathrm{a})}(\mathbf{r}) = u^2(\mathbf{r}) \begin{bmatrix} 0 & \epsilon_x\epsilon_y \sin\delta & 0 \\ -\epsilon_x\epsilon_y \sin\delta & 0 & 0 \\ 0 & 0 & 0 \end{bmatrix} \tag{4.3b}$$

are, respectively, the symmetric and antisymmetric components of the Maxwell stress tensor, and where we have decomposed the polarization into Cartesian components,

$$\hat{\epsilon} = \epsilon_x \hat{x} + \mathrm{e}^{\mathrm{i}\delta}\epsilon_y \hat{y}. \tag{4.4}$$

The symbol $\Im\{\cdot\}$ represents the imaginary part of its argument. A right-circularly polarized beam of light has $\delta = \pi/2$ and a linearly polarized beam has $\delta = 0$. Although equation (3.4) for $\mathbf{F}_{\mathrm{e}}(\mathbf{r})$ accounts only for the electric dipole contribution and should be augmented by the analogous result for the magnetic dipole contribution, equation (4.2) for $\mathbf{F}_{\mathrm{em}}(\mathbf{r})$ includes both electric and magnetic contributions.

(a) Linear polarization: trap anisotropy

For small dielectric particles, the intensity-gradient contribution from equation (4.2*a*) tends to strengthen the trap, and the phase-gradient contribution from equation (4.2*b*) tends to diminish radiation pressure. The symmetric part of $\mathcal{T}(\mathbf{r})$ contributes to the force exerted by linearly polarized optical tweezers, and tends to weaken the trap along the direction of polarization. Lateral anisotropy in optical tweezers' trapping stiffness has been observed in both experimental and numerical studies [13,27]. Equation (4.2*c*) suggests that this effect should be reversed for magneto-dielectric Rayleigh particles satisfying $\Im\{\alpha_{\mathrm{e}}\alpha_{\mathrm{m}}^*\} < 0$.

(b) Circular polarization: spin-curl forces

The antisymmetric part of $\mathcal{T}(\mathbf{r})$ comes to the fore in circularly polarized optical tweezers, contributing forces and torques involving light's angular momentum. Light's spin angular momentum contributes to photokinetic forces through the relationship [17]

$$\nabla \cdot \mathcal{T}^{(\mathrm{a})} = \frac{\omega}{\epsilon} \nabla \times \mathbf{s}(\mathbf{r}), \tag{4.5}$$

where

$$\mathbf{s}(\mathbf{r}) = \frac{\epsilon}{2\omega} \Im\{\mathbf{E}^*(\mathbf{r}, t) \times \mathbf{E}(\mathbf{r}, t)\} \tag{4.6}$$

is the time-averaged spin angular momentum density carried by the beam [38–42]. In the paraxial model for circularly polarized optical tweezers,

$$\mathbf{s}(\mathbf{r}) \approx \pm \frac{\epsilon}{2\omega} u^2(\mathbf{r}) \hat{z}, \tag{4.7}$$

where the positive choice corresponds to right-circular polarization. The associated spin-curl [9, 14] contribution to the photokinetic force,

$$\mathbf{F}_{\mathrm{em}}^{(\mathrm{a})}(\mathbf{r}) = \mp \frac{\epsilon k^3}{12\pi\epsilon_0} \Re\{\alpha_{\mathrm{e}}\alpha_{\mathrm{m}}^*\} \partial_r u^2(\mathbf{r}) \hat{\theta}, \tag{4.8}$$

tends to drive the particle around the optical axis in the right-handed sense for right-circularly polarized light (−) and in the opposite direction for left-circularly polarized light (+). This effect also has been observed experimentally [13].

Figure 3*a*,*b* presents streamlines of the calculated dipole-order optical force, including $\mathbf{F}_{\mathrm{em}}(\mathbf{r})$ exerted by a Gaussian beam focused at NA = 1.2 on a 100 nm diameter silica sphere dispersed in water. The trap is indicated in these illustrations by the shaded profile and propagates upward along $\hat{z}$. The spin-curl contribution amounts to just 3% of the total optical force, but still suffices to impart a clear twist to the force field. The magnitude of this effect can be appreciated by comparing the results for right- and left-circularly polarized light in figure 3*a*,*b*, respectively.

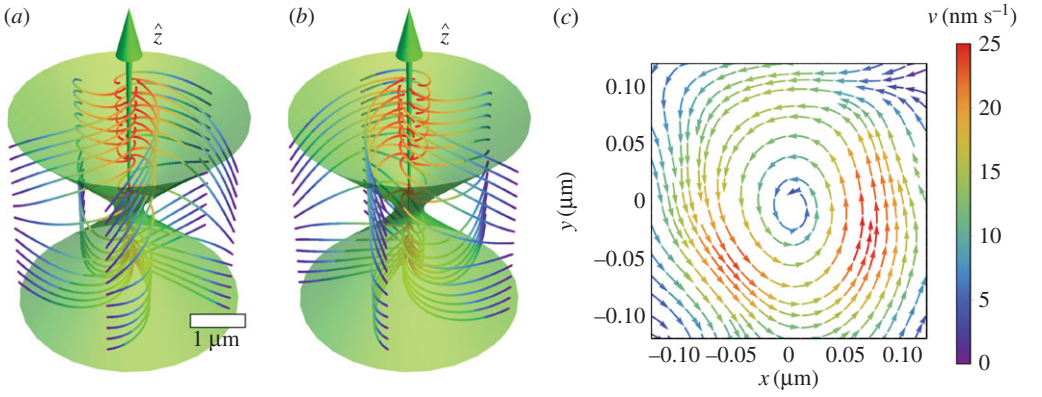

Figure 3. Photokinetic forces in circularly polarized optical tweezers exert torques about the optical axis. (*a*) Streamlines of the force field for a right-circularly polarized optical tweezer, computed with equations (3.5) and (4.8) for a 100 nm diameter silica sphere in a trap formed at NA = 1.2. (*b*) Equivalent result for a left-circularly polarized trap. (*c*) Streamlines of the experimentally measured circulation of a 1 μm diameter polystyrene sphere localized in a right-circularly polarized trap. (Online version in colour.)

More generally, the spin-curl term described by equation (4.2*d*) gives rise to an azimuthal force that is proportional to the degree of circular polarization. This is consistent with experimental observations of colloidal spheres circulating around the optical axis in such traps [13,43]. This effect is noteworthy because it constitutes an optical torque arising from light's spin angular momentum that acts on small objects even if they are optically isotropic.

Figure 3*c* presents experimental data, originally discussed in Ruffner & Grier [13], for a 1 μm diameter polystyrene sphere diffusing in the force field created by a right-circularly polarized optical tweezer. Although the present theory is intended for smaller particles, a sphere of this size can be tracked with nanometre precision using holographic video microscopy [13,44]. This resolution is fine enough to resolve the subtle influence of spin-curl forces. The data in figure 3*c* were compiled from 7000 location measurements at 33 ms intervals. These trajectory data were used to estimate the local velocity field, $\mathbf{v}(\mathbf{r})$, whose streamlines are plotted in the transverse plane passing through the trap's equilibrium position. Right-handed circulation is clearly evident, with a peak drift speed of 25 nm s^{-1}. The apparent spiralling of the streamlines is an artefact of the finite spatial resolution of the measurement.

The observed circulation represents a very slight bias on the particle's Brownian motion. In the absence of thermal forces, the particle would remain stationary at the trap's equilibrium point. The data in figure 3*c*, therefore, reveal another example of a Brownian vortex, this one governed by the light's polarization.

Unlike the toroidal roll from figure 2, the Brownian vortex driven by spin-curl forces takes the form of a rotating cloud of probability. Its circulation reveals a net transfer of angular momentum from the circularly polarized beam of light to the mechanical system. This is striking because every element of the system is optically isotropic. The torque emerges from the influence of the light's non-uniform magnetic field on the particle's oscillating electric dipole moment [36], and would not arise in a uniform beam of light.

Spin-curl forces superficially resemble the forces arising from light's orbital angular momentum. Both act transverse to the optical axis and can transfer angular momentum to illuminated objects. Orbital angular momentum acts through phase gradients in the canted wavefronts of helical modes of light; its influence arises at first order and is proportional to the local intensity. Spin-curl forces, by contrast, arise at second order and are directed by intensity gradients. Because they operate in the paraxial approximation, however, spin-curl forces should be no less influential than spin-to-orbital conversion, which emerges only in strongly converging

beams [9,11]. For published experimental studies on micrometre-scale colloidal spheres [13], the spin-curl contribution is found to dominate.

For particles smaller than the wavelength of light, higher-order multipole contributions are weaker than the dipole-order terms that we have discussed. These terms' symmetries offer insights into the nature of their contributions. Independent multipole terms, for example, are symmetric under exchange of the fields' components. They cannot describe spin-dependent effects, therefore, because the spin angular momentum density is antisymmetric. Additional spin-dependent terms can arise from interference between multipole contributions. These contributions may be negligible for Rayleigh particles. For larger particles, however, they might provide additional avenues for optical micromanipulation under control of light's angular momentum.

5. Conclusion

The theory of photokinetic effects expresses optical forces and torques in terms of the amplitude and phase profiles of a beam of light within the framework of the conventional multipole expansion. Its goal is to elucidate relationships among experimentally accessible characteristics of the beam of light and the resulting landscape of forces and torques experienced by small illuminated objects. We have applied this methodology to the illustrative case of optical tweezers acting on Rayleigh particles in the paraxial approximation. Even this idealized model captures such subtle features as the trap's polarization-dependent anisotropy. It also clarifies the mechanism by which light's spin angular momentum induces a measurable force on small objects even when those objects are optical isotropic. In the case of circularly polarized optical tweezers, this force is solenoidal and causes objects to circulate around the optical axis. This behaviour is reminiscent of the motion induced by transfer of orbital angular momentum from helical beams of light, but arises from the curl of the spin angular momentum density rather than the gradient of the phase.

Beyond explaining the performance of existing optical traps, photokinetic analysis offers guidance for designing new modes of light specially suited for optical micromanipulation. It promises to be particularly useful for crafting extended landscapes of force and torque through which illuminated objects can move. These landscapes can feature all of the influences that light can exert, including those arising from light's intrinsic and extrinsic angular momentum.

Authors' contributions. D.J.E. proposed the project and initiated the calculation of dipole-level forces. D.G.G. and A.Y. performed the remaining calculations and wrote the paper.

Data accessibility. Data for this study can be accessed online at http://physics.nyu.edu/grierlab/ or by contacting the corresponding author.

Competing interests. The authors have no competing interests.

Funding. This work was supported primarily by NASA through Award no. NNX13AK76G and through the NASA Space Technology Research Fellowship (NSTRF) program under Award no. NN14AQ40H. Partial support was provided by the Materials Research Science and Engineering program of the National Science Foundation under Award no. DMR-1420073.

References

1. Beth RA. 1935 Direct detection of the angular momentum of light. *Phys. Rev.* **48**, 471. (doi:10.1103/PhysRev.48.471)
2. Allen L, Beijersbergen MW, Spreeuw RJC, Woerdman JP. 1992 Orbital angular-momentum of light and the transformation of Laguerre–Gaussian laser modes. *Phys. Rev. A* **45**, 8185–8189. (doi:10.1103/PhysRevA.45.8185)
3. He H, Friese MEJ, Heckenberg NR, Rubinsztein-Dunlop H. 1995 Direct observation of transfer of angular momentum to absorptive particles from a laser beam with a phase singularity. *Phys. Rev. Lett.* **75**, 826–829. (doi:10.1103/PhysRevLett.75.826)
4. Simpson NB, Allen L, Padgett MJ. 1996 Optical tweezers and optical spanners with Laguerre–Gaussian modes. *J. Mod. Opt.* **43**, 2485–2491. (doi:10.1080/09500349608230675)

5. Gahagan KT, Swartzlander GA. 1996 Optical vortex trapping of particles. *Opt. Lett.* **21**, 827–829. (doi:10.1364/OL.21.000827)
6. Padgett M, Bowman R. 2011 Tweezers with a twist. *Nat. Photon.* **5**, 343–348. (doi:10.1038/nphoton.2011.81)
7. Andrews DL, Babiker M. (eds). 2013 *The angular momentum of light*. New York, NY: Cambridge University Press.
8. Roichman Y, Sun B, Roichman Y, Amato-Grill J, Grier DG. 2008 Optical forces arising from phase gradients. *Phys. Rev. Lett.* **100**, 013602. (doi:10.1103/PhysRevLett.100.013602)
9. Zhao YQ, Edgar JS, Jeffries GDM, McGloin D, Chiu DT. 2007 Spin-to-orbital angular momentum conversion in a strongly focused optical beam. *Phys. Rev. Lett.* **99**, 073901. (doi:10.1103/PhysRevLett.99.073901)
10. Wang XL, Chen J, Li YN, Ding JP, Guo CS, Wang HT. 2010 Optical orbital angular momentum from the curl of polarization. *Phys. Rev. Lett.* **105**, 253602. (doi:10.1103/PhysRevLett.105.253602)
11. Marrucci L, Karimi E, Slussarenko S, Piccirillo B, Santamato E, Nagali E, Sciarrino F. 2011 Spin-to-orbital conversion of the angular momentum of light and its classical and quantum applications. *J. Opt.* **13**, 064001. (doi:10.1088/2040-8978/13/6/064001)
12. Cipparrone G, Ricardez-Vargas I, Pagliusi P, Provenzano C. 2010 Polarization gradient: exploring an original route for optical trapping and manipulation. *Opt. Express* **18**, 6008–6013. (doi:10.1364/OE.18.006008)
13. Ruffner DB, Grier DG. 2012 Optical forces and torques in non-uniform beams of light. *Phys. Rev. Lett.* **108**, 173602. (doi:10.1103/PhysRevLett.108.173602)
14. Albaladejo S, Marqués MI, Laroche M, Sáenz JJ. 2009 Scattering forces from the curl of the spin angular momentum. *Phys. Rev. Lett.* **102**, 113602. (doi:10.1103/PhysRevLett.102.113602)
15. Ruffner DB, Grier DG. 2013 Comment on 'Scattering forces from the curl of the spin angular momentum of a light field'. *Phys. Rev. Lett.* **111**, 059301. (doi:10.1103/PhysRevLett.111.059301)
16. Bekshaev AY, Bliokh KY, Nori F. 2015 Transverse spin and momentum in two-wave interference. *Phys. Rev. X* **5**, 011039. (doi:10.1103/PhysRevX.5.011039)
17. Yevick A, Ruffner DB, Grier DG. 2016 Tractor beams in the Rayleigh limit. *Phys. Rev. A* **93**, 043807. (doi:10.1103/PhysRevA.93.043807)
18. Nieminen TA, Loke VLY, Stilgoe AB, Knoner G, Branczyk AM, Heckenberg NR, Rubinsztein-Dunlop H. 2007 Optical tweezers computational toolbox. *J. Opt. A* **9**, S196–S203. (doi:10.1088/1464-4258/9/8/S12)
19. Sun B, Roichman Y, Grier DG. 2008 Theory of holographic optical trapping. *Opt. Express* **16**, 15765–15776. (doi:10.1364/OE.16.015765)
20. Ashkin A, Dziedzic JM, Bjorkholm JE, Chu S. 1986 Observation of a single-beam gradient force optical trap for dielectric particles. *Opt. Lett.* **11**, 288–290. (doi:10.1364/OL.11.000288)
21. Born M, Wolf E. 1999 *Principles of optics*, 7th edn. Cambridge, UK: Cambridge University Press.
22. Draine BT, Goodman J. 1994 Beyond Clausius–Mossotti: wave propagation on a polarizable point lattice and the discrete dipole approximation. *Astrophys. J.* **405**, 685–697. (doi:10.1086/172396)
23. Albaladejo S, Gómez-Medina R, Froufe-Pérez LS, Marinchio H, Carminati R, Torrado JF, Armelles G, García-Martin A, Sáenz JJ. 2010 Radiative corrections to the polarizability tensor of an electrically small anisotropic dielectric particle. *Opt. Express* **18**, 3556–3567. (doi:10.1364/OE.18.003556)
24. Chaumet PC, Nieto-Vesperinas M. 2000 Time-averaged total force on a dipolar sphere in an electromagnetic field. *Opt. Lett.* **25**, 1065–1067. (doi:10.1364/OL.25.001065)
25. Tlusty T, Meller A, Bar-Ziv R. 1998 Optical gradient forces of strongly localized fields. *Phys. Rev. Lett.* **81**, 1738–1741. (doi:10.1103/PhysRevLett.81.1738)
26. Florin EL, Pralle A, Stelzer EHK, Horber JKH. 1998 Photonic force microscope calibration by thermal noise analysis. *Appl. Phys. A* **66**, S75–S78. (doi:10.1007/s003390051103)
27. Rohrbach A. 2005 Stiffness of optical traps: quantitative agreement between experiments and electromagnetic theory. *Phys. Rev. Lett.* **95**, 168102. (doi:10.1103/PhysRevLett.95.168102)
28. Ruffner DB, Grier DG. 2014 Universal, strong and long-ranged trapping by optical conveyors. *Opt. Express* **22**, 26 834–26 853. (doi:10.1364/OE.22.026834)
29. Madadi E, Samadi A, Cheraghian M, Reihani NS. 2012 Polarization-induced stiffness asymmetry of optical tweezers. *Opt. Lett.* **37**, 3519–3521. (doi:10.1364/OL.37.003519)

30. Roichman Y, Sun B, Stolarski A, Grier DG. 2008 Influence of non-conservative optical forces on the dynamics of optically trapped colloidal spheres: the fountain of probability. *Phys. Rev. Lett.* **101**, 128301. (doi:10.1103/PhysRevLett.101.128301)
31. Sun B, Lin J, Darby E, Grosberg AY, Grier DG. 2009 Brownian vortexes. *Phys. Rev. E* **80**, 010401(R). (doi:10.1103/PhysRevE.80.010401)
32. Khan M, Sood AK. 2011 Tunable Brownian vortex at the interface. *Phys. Rev. E* **83**, 041408. (doi:10.1103/PhysRevE.83.041408)
33. Sun B, Grier DG, Grosberg AY. 2010 Minimal model for Brownian vortexes. *Phys. Rev. E* **82**, 021123. (doi:10.1103/PhysRevE.82.021123)
34. Moyses H, Bauer RO, Grosberg AY, Grier DG. 2015 Perturbative theory for Brownian vortexes. *Phys. Rev. E* **91**, 062144. (doi:10.1103/PhysRevE.91.062144)
35. Gordon JP. 1973 Radiation forces and momenta in dielectric media. *Phys. Rev. A* **8**, 14–21. (doi:10.1103/PhysRevA.8.14)
36. Rahmani PC, Chaumet A. 2009 Electromagnetic force and torque on magnetic and negative-index scatterers. *Opt. Express* **17**, 2224–2234. (doi:10.1364/OE.17.002224)
37. Schonbrun E, Crozier KB. 2008 Spring constant modulation in a zone plate tweezer using linear polarization. *Opt. Lett.* **33**, 2017–2019. (doi:10.1364/OL.33.002017)
38. Barnett SM. 2002 Optical angular-momentum flux. *J. Opt. B* **4**, S7–S16. (doi:10.1088/1464-4266/4/2/361)
39. Berry MV. 2009 Optical currents. *J. Opt. A* **11**, 094001. (doi:10.1088/1464-4258/11/9/094001)
40. Berry MV, Dennis MR. 2001 Polarization singularities in isotropic random vector waves. *Proc. R. Soc. Lond. A* **457**, 141–155. (doi:10.1098/rspa.2000.0660)
41. Bekshaev A, Bliokh KY, Soskin M. 2011 Internal flows and energy circulation in light beams. *J. Opt.* **13**, 053001. (doi:10.1088/2040-8978/13/5/053001)
42. Bliokh K, Dressel J, Nori F. 2014 Conservation of the spin and orbital angular momentum in electromagnetism. *New J. Phys.* **16**, 093037. (doi:10.1088/1367-2630/16/9/093037)
43. Friese MEJ, Nieminen TA, Heckenberg NR, Rubinsztein-Dunlop H. 1998 Optical torque controlled by elliptical polarization. *Opt. Lett.* **23**, 1–3. (doi:10.1364/OL.23.000001)
44. Lee SH, Roichman Y, Yi GR, Kim SH, Yang SM, van Blaaderen A, van Oostrum P, Grier DG. 2007 Characterizing and tracking single colloidal particles with video holographic microscopy. *Opt. Express* **15**, 18 275–18 282. (doi:10.1364/OE.15.018275)